Available online at www.sciencedirect.com
SCIENCE DIRECT
Journal of Organometallic Chemistry 691 (2006) 1998–2004
Journal of Organometallic Chemistry
www.elsevier.com/locate/jorganchem

Synthesis, characterization and electroluminescence of B(III) compounds: BPh_2(2-(2-quinolyl)naphtho[*b*]imidazolato) and BPh_2(2-(2-quinolyl)benzimidazolato)

Tsun-Ren Chen [a,*], Rong-Hong Chien [b], Anchi Yeh [b], Jhy-Der Chen [c]

[a] *Department of Electrical Engineering, Yung-Ta Institute of Technology, Ping-Tung, Taiwan, ROC*
[b] *Department of Chemical Engineering, Chengshiu University, Kaohsiung, Taiwan, ROC*
[c] *Department of Chemistry, Chung-Yuan Christian University, Chung-Li, Taiwan, ROC*

Received 31 August 2005; received in revised form 26 December 2005; accepted 27 December 2005
Available online 14 February 2006

Abstract

Two novel luminescent boron compounds, BPh_2(2-(2-quinolyl)naphtho[*b*]imidazolato) (**1**) and BPh_2(2-(2-quinolyl)benzimidazolato) (**2**), have been synthesized by the reactions of triphenylboron with appropriate ligands, 2-(2-quinolyl)naphtho[*b*]imidazole (QNI) and 2-(2-quinolyl)benzimidazole (QBI), respectively. The structure of **1** was determined by single crystal X-ray diffraction, while **2** by spectroscopic methods. The structure of **1** reveals that the boron center is four coordinated. Several types of OLED possessing different colors were fabricated by using **1** as emitter. For the three-layer OLED with the structure ITO/NPB/**2**/Alq_3/Mg–Ag, an emission band covering the whole visible region from 400 to 750 nm with the maximum brightness of 320 cd/m^2 was observed, indicating a perfect white light OLED (CIE = 0.33, 0.37). Compounds **1** and **2** form a new family of organometallic emitting materials which could be of interest for practical application.

Keywords: Excimer; White light; Electroluminescence; Imidazole; Boron; Intermolecular charge transfer

1. Introduction

The chemistry of organoboron compounds have attracted much more attention recently because they are of interest for practical applications [1–3]. Since an organic light emitting diode (OLED) was reported by Tang and Vanslyke [4], LEDs based on organic materials have generated considerable interest and enabled the development of low-cost, full-color, flat-panel displays [5–8]. The best-known EL metal complex used in OLED is Alq_3 which is not only a good emitter but also a highly efficient electron-transporting material, where *q* is the 8-hydroxyquinolinato ligand [9,10]. Via the modification of the ligands of metal complexes, the emission spectra of devices and other properties, such as thermo stability and carrier mobility, can be tuned. The imidazoles have been known as good chelating ligands [11] and the attachment of the quinolyl group at 2-position of imidazoles would allow the new ligands to form stable compounds with the other atoms. In the present work, the syntheses, structures, and electroluminescent properties of two new boron compounds BPh_2(2-(2-quinolyl)naphtho[*b*]imidazolato) (**1**) and BPh_2-(2-(2-quinolyl)benzimidazolato) (**2**) are reported.

2. Results and discussion

2.1. Syntheses and characterization

The two new boron compounds BPh_2(2-(2-quinolyl)-naphtho[*b*]imidazolato) (**1**) and BPh_2(2-(2-quinolyl)benz-

* Corresponding author. Tel./fax: +886 8 7333632.
E-mail address: trchen@mail.ytit.edu.tw (T.-R. Chen).

0022-328X/$ - see front matter © 2006 Elsevier B.V. All rights reserved.
doi:10.1016/j.jorganchem.2005.12.060

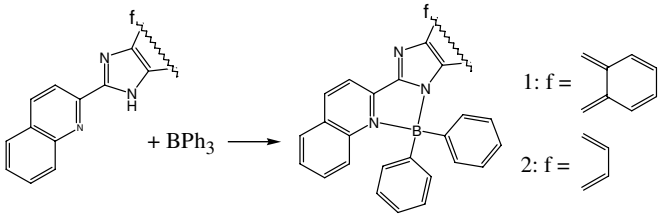

Scheme 1.

imidazolato) (**2**) were prepared by reacting triphenylboron with appropriate imidazole in dry THF (Scheme 1). Both the compounds are air-stable in the solid state and in solution. The thermogravimetric analyses (TGA) scans under nitrogen for **1** and **2** powders showed weight loss of 10% at 333 and 326 °C, respectively, which reveals that both of **1** and **2** are quite stable in the atmosphere of nitrogen. The DSC results indicate that both of the compounds **1** and **2** possess a very high melting temperatures, 220 and 298 °C, respectively, which may serve as an advantage for OLED device fabrication because the materials having high transition temperature could provide the device with greater longevity [12,13].

2.2. Structure of *1*

Single crystals of **1** were grown by slow diffusion of hexane into a concentrated solution of **1** in dichloromethane. The molecular structure of **1** is shown in Fig. 1 and the selected bond lengths and angles are listed in Table 1. In this structure, the boron atom in **1** has a typical tetrahedral geometry. The QNI is bidentately chelated to the boron center through its quinolyl and imidazole nitrogen atoms, and two phenyl groups occupy the other boron sites. The bond length of B–N(2) imidazole bond (1.567(5) Å) is shorter than that of the B–N(1) quinolyl bond (1.659(5) Å), indicating that the imidazole nitrogen is anionic and hence a better donor than the neutral quinolyl nitrogen atom [2]. The two five-membered rings are nearly coplanar with a dihedral angle of 5.8° between these two rings. Fig. 2 shows a packing diagram for **1**. The interplanar distances between imidazol ring and quinolyl moiety are in the range of 3.3–3.6 Å, which implies that the intermolecular charge transfer interaction (ICT) may play an important role in producing face-to-face π–π stacking interaction [14].

Table 1
Selected bond distance (Å) and angles (°) for **1**

Bond distance			
B–N(2)	1.567(5)	B–C(27)	1.599(5)
B–C(21)	1.621(5)	B–N(1)	1.659(5)
N(1)–C(1)	1.335(4)	N(1)–C(9)	1.376(4)
N(2)–C(20)	1.365(4)	N(2)–C(10)	1.382(4)
N(3)–C(20)	1.309(4)	N(3)–C(19)	1.398(4)
Bond angles			
N(2)–B–C(27)	110.7(3)	N(2)–B–C(21)	112.8(3)
C(27)–B–C(21)	117.8(3)	N(2)–B–N(1)	94.4(2)
C(27)–B–N(1)	113.7(3)	C(21)–B–N(1)	104.9(3)
C(1)–N(1)–C(9)	120.0(3)	C(1)–N(1)–B	111.8(3)
C(9)–N(1)–B	127.8(3)	C(20)–N(2)–C(10)	104.5(3)
C(20)–N(2)–B	113.6(3)	C(10)–N(2)–B	141.7(3)
C(20)–N(3)–C(19)	102.2(3)		

2.3. Electronic absorption and photoluminescence spectra

The thin films of **1** and **2** used for the analyses of UV–Vis and photoluminescence spectra were obtained by depositing **1** and **2** onto quartz substrates under vacuum condition.

At room temperature and low concentration (1×10^{-7} M), the absorption spectral features of **1** and **2** in *N*,*N*′-dimethylformamide (DMF) consist of two discrete bands (Figs. 3 and 4). The strong absorptions centered at

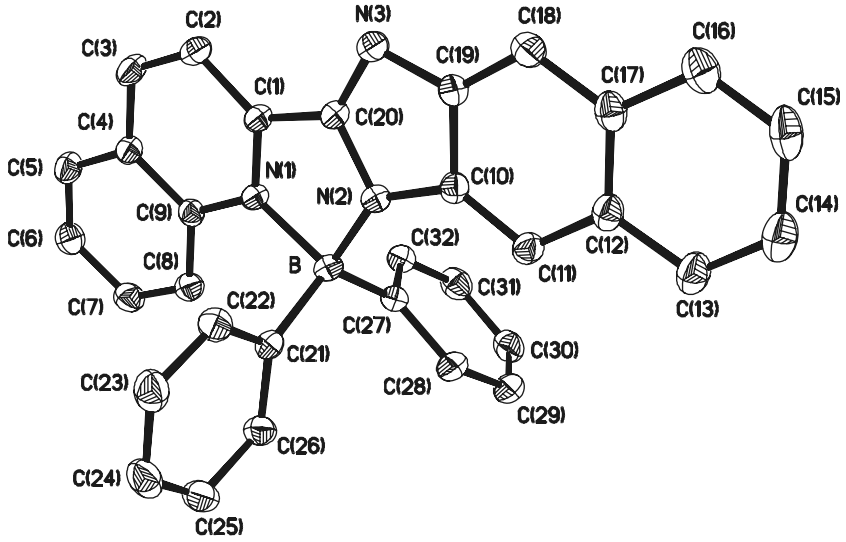

Fig. 1. ORTEP drawing of the molecular structure of complex **1**. Ellipsoids are scaled to enclose 20% of electron density.

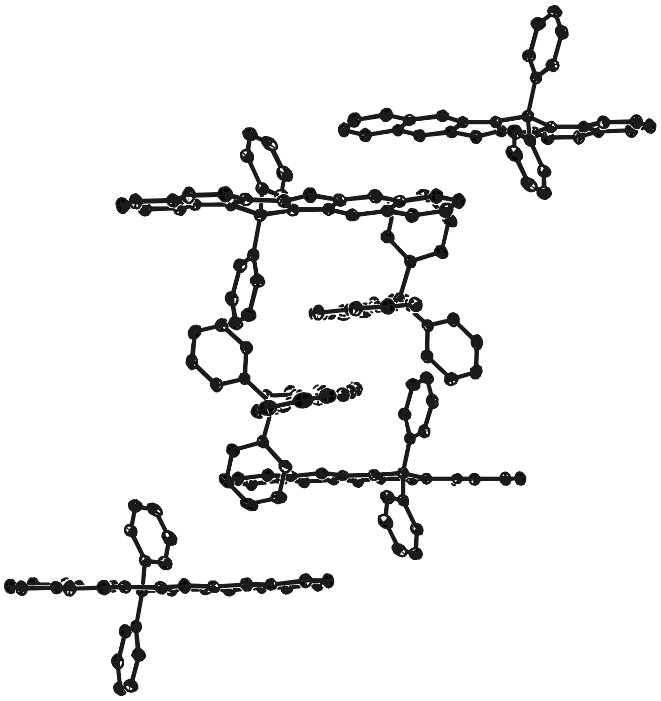

Fig. 2. An illustration of the stacking present in crystal **1**.

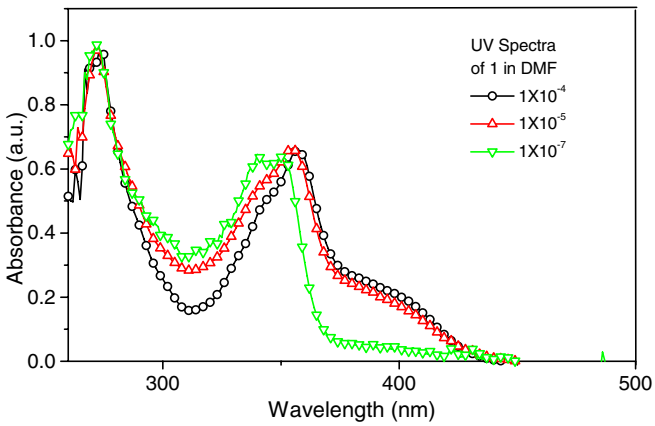

Fig. 3. UV–Vis spectra of **1** in *N*,*N*′-dimethylformamide.

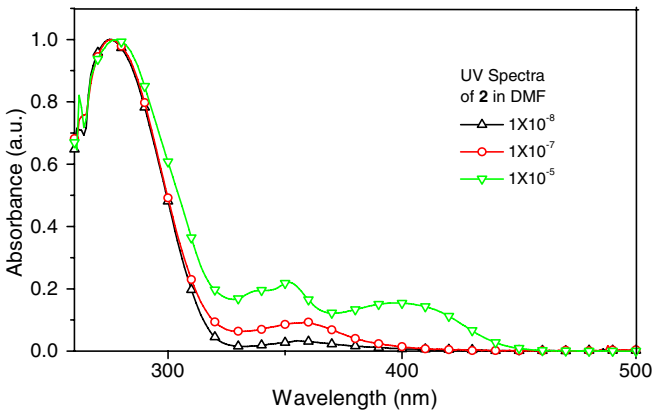

Fig. 4. UV–Vis spectra of **2** in *N*,*N*′-dimethylformamide.

272 and 278 nm for **1** and **2**, respectively, can be assigned to the π–π^* transition. The other intense band centered at 351 nm shows a vibrational separation of 1000 cm^{-1} with the $v_{0,0}$ transition at 2.94×10^3 cm^{-1}. This lower energy band possesses a reasonably high absorptivty ($\varepsilon \sim 3 \times 10^4$ dm^3 mol^{-1} cm^{-1}) and a red shift with increasing polarity of solvent, which is typical for a π–π^* transition [15,16]. When the solutions became more concentrated, a new absorbing band in a range of 370–450 nm appeared, which are consistent with the intermolecular charge transfer (ICT) character for the concerned π–π^* transition involving the filled π orbital (HOMO) located on the imidazol ring and the unoccupied π^* orbital (LUMO) located on the quinoly ring [17–21]. Comparing the absorption spectra of **1** and **2** with the ligands QNI and QBI, the absorption bands of **1** and **2** are almost identical to the ligands, which reveal that the electronic transitions of **1** and **2** are localized on the ligands QNI and QBI [22].

Figs. 5 and 6 show the photoluminescence (PL) spectra of the solutions and neat film of **1** and **2**, excited with 355 nm laser line. At low concentration, 1×10^{-8} M in

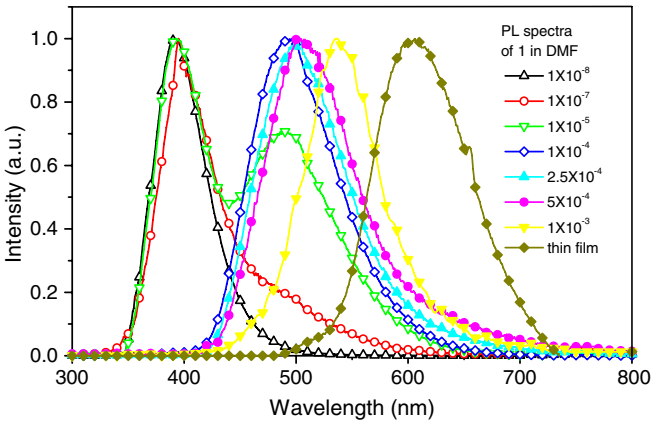

Fig. 5. Photoluminescence spectra of t complex **1** in various concentrations and neat film, excited with 355 nm laser line.

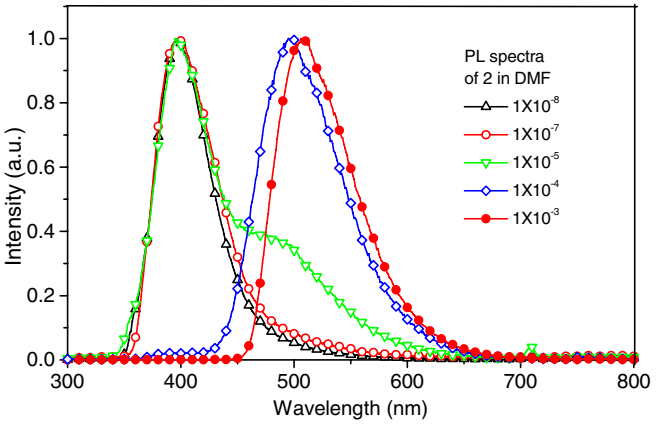

Fig. 6. Photoluminescence spectra of complex **2** in various concentrations, excited with 355 nm laser line.

DMF, only one emission band was observed with a maximum at 395 nm, which corresponds to the relaxation of **1** or **2** from the excited state of a single molecule into ground state. Interestingly, when the concentration were increased to 1×10^{-5} M, a new emission band having a maximum at 495 nm was observed, which can be attributed to the formation of excimers by exciting monomers that happened to be in ground-state [23,24]. When the solution became more concentrated, reaching 1×10^{-4} M, the monomer emission disappeared and only the excimer emission existed. Furthermore, when the concentration was increased further, the emission band moved toward the longer wavelength and reached a maximum number (610 nm) in solid state (thin film), which could be attributed to the self-association of molecules [14]. It is noticeable that the peak emission wavelengths of **1** and **2** cover the full range of visible region from blue to red, which is a promising character for the application of organic light emitting displays, especially for white OLEDs. Compounds **1** and **2** possess the appreciable PL quantum yield, with $\Phi_f = 0.15$ and 0.46, respectively, 10^{-6} M in DMF relative to 3-(2-benzothiazolyl)-7-diethyl-aminocoumarin (C540).

2.4. Electroluminescence studies

In order to evaluate the electroluminescence characteristics of compounds **1** and **2**, various EL devices were constructed as shown in Fig. 7. The EL devices using **1** or **2** as emitters were fabricated on the transparent conductive indium-tin oxide (ITO) glass substrates cleaned by detergent solution and deionized water and dried by organic solvent vapor. The organic layers and the cathode were sequentially deposited by conventional vacuum-vapor deposition in the same chamber without breaking the vacuum under 3×10^{-6} Torr. The cathode composed of magnesium silver alloy (Mg:Ag = 10:1) was deposited onto the top layer of organic materials by co-evaporation of Mg and Ag from different source. Before the deposition, all of the organic materials were purified by a train sublimation method. Molecular structures of the organic materials used in this study are shown in Fig. 8. *N*,*N*′-bis-(1-naphthyl)-*N*,*N*′-diphenyl-1,1′-biphenyl-4,4′-diamine (NPB) was used as a hole-transport material (HTM), and tris(8-quinnolinolato) aluminum (Alq_3) was employed as an electron-transporting material (ETM). The thickness of the organic layers and cathode were measured by quartz-crystal monitor.

Fig. 7a shows a two-layer OLED possessing NPB as an HTM and **1** as an emitter (device A). The EL spectrum of this device, Fig. 9, is similar to the PL spectrum of **1** in solid state. From the energy diagram of the materials used in this work, Fig. 10, it can be seen that because the relatively large gap between the LUMO of complex **1** and the work function of cathode is quite high, the device current should

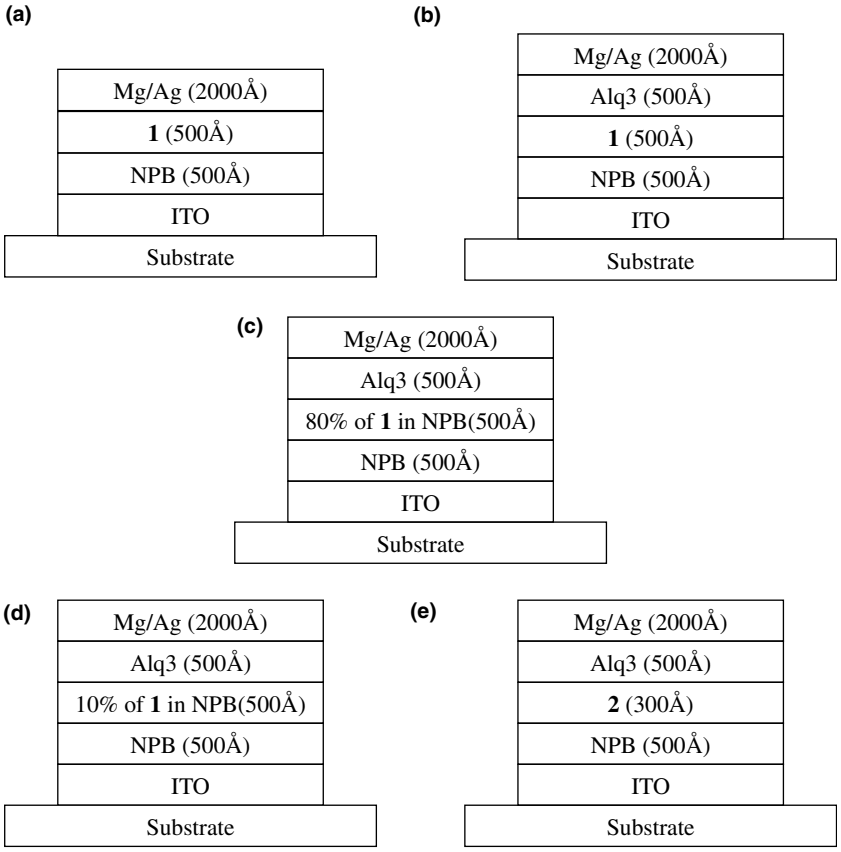

Fig. 7. The EL device structures fabricated in this work.

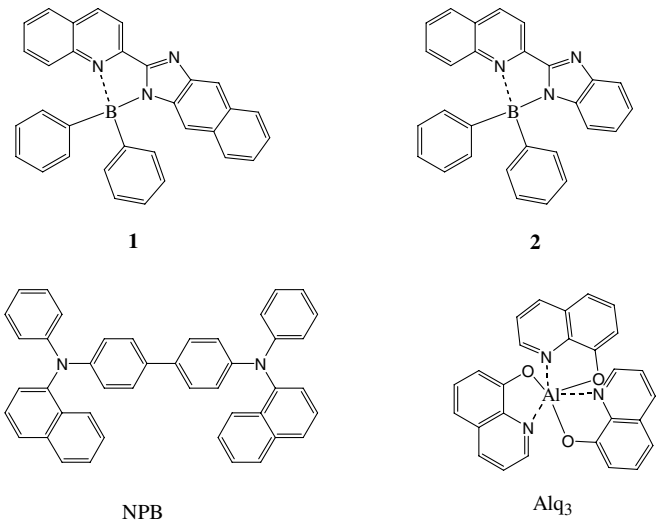

Fig. 8. Molecular structures of BPh_2(2-(2-quinolyl)naphtho[*b*]imidazolato) **(1)**, BPh_2(2-(2-quinolyl)benzimidazolato) **(2)**, *N*,*N*′-bis-(1-naphthyl)-*N*,*N*′-diphenyl-1,1′-biphenyl-4,4′-diamine (NPB), and tris(8-quinnolinolato) aluminum (Alq_3).

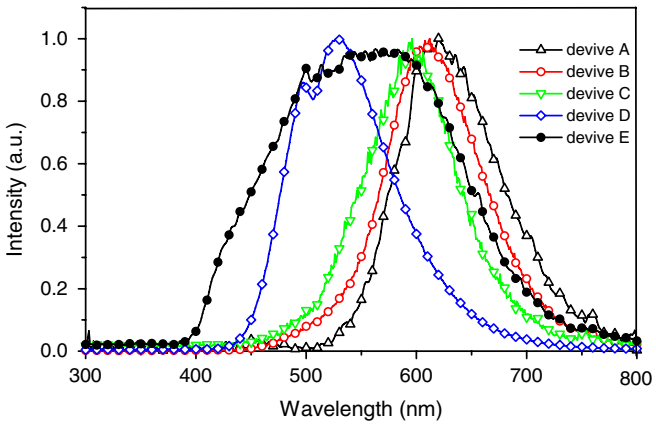

Fig. 9. The EL spectra of devices A–E.

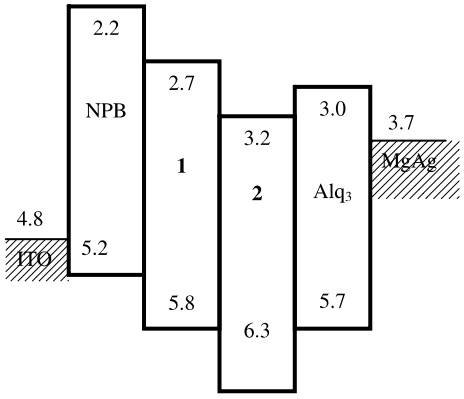

Fig. 10. The energy level diagram of materials used in this work.

be dominated by holes and light emission should originate from the emitter/cathode interface [25] in which the density of **1** is very high. As the photoluminescence characteristics of **1** in thin film, the self-association of **1** in device A forms a metastable species. Such electronically excited species produce the long wavelength of light [26]; therefore a red emission (EL peak = 618 nm, CIE coordinates $x = 0.66$ and $y = 0.32$) was obtained. The voltage–current density characteristic of device A, Fig. 11, reveals that the resistance of this device is quite high. In addition, the carrier recombination takes place close to cathode, which would not only damage the electrode but also reduce the light output so that the luminance of this device is relatively low, Fig. 12.

Fig. 7b shows a three-layer OLED (device B). In this device, the Alq_3 was employed as an ETM to lower the electron injection barrier at the cathode/emitter interface. For device B, an EL spectrum having a peak emission wavelength at 608 nm was observed, which is shorter by 10 nm than that of device A, which reveals that the carrier recombination zone would be confined at the Alq_3/complex **1** interface in which complex **1** was partially mixed with Alq_3. The voltage–current density characteristic of device B, Fig. 12, shows that the barrier of Alq_3/complex **1** interface was expectantly reduced by the addition of ETM, and the EL efficiency was improved.

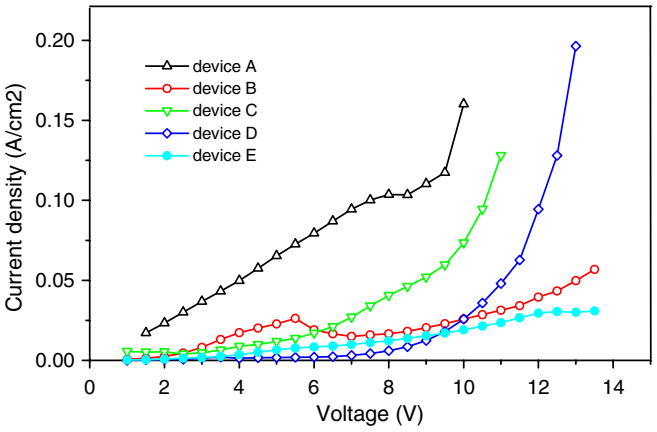

Fig. 11. The current–voltage characteristics of devices A–E.

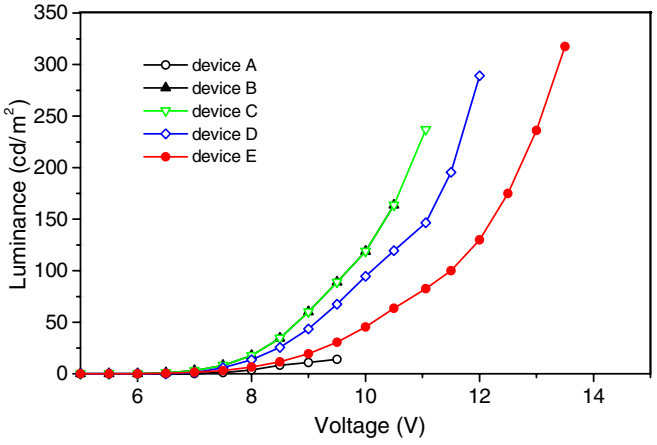

Fig. 12. The luminance–voltage characteristics of devices A–E.

Fig. 7c shows a three-layer OLED with the configuration ITO/NPB/NPB + complex **1** (80 wt%)/Alq_3/Mg–Ag (device C). Fig. 9 shows the EL spectra of this device having an emission maximum at 596 nm. Comparing to device A and B, the emission band of this device was apparently shifted to a shorter wavelength, and an orange OLED (coordinates $x = 0.52$ and $y = 0.48$) was obtained.

Fig. 7d shows a three-layer OLED with the configuration ITO/NPB/NPB + complex **1** (10 wt%)/Alq_3/Mg–Ag (device D). Fig. 9 shows the EL spectra of this device having an emission maximum at 526 nm. Interestingly, the emission wavelength of this device became much shorter, and a yellow OLED (coordinates $x = 0.47$ and $y = 0.50$) was obtained.

Fig. 7e shows a three-layer OLED with the structure ITO/NPB/**2**/Alq_3/Mg–Ag (device E). According to the energy diagram, Fig. 10, the LUMO level of **2** is lower than that of Alq_3, which suggests that the electron will be easy to transfer from Alq_3 to emitter, so the recombination zone will not be confined at the Alq_3/emitter interface, but be located in the emitting layer; therefore, an emission band covering the whole visible region from 400 to 750 nm with the maximum brightness of 320 cd/m^2 was observed, and a perfect white light OLED (CIE = 0.33, 0.37) was obtained.

3. Concluding remarks

A new family of emitter for OLED, BPh_2(2-(2-quinolyl)-naphtho[*b*]imidazolato) (**1**) and BPh_2(2-(2-quinolyl)benzimidazolato) (**2**), have been successfully synthesized and investigated. It has been shown that the novel ligands QNI and QBI are capable of chelating to B(III) centers and the resulting compounds possess appreciable photoluminescent efficiency and very high thermal stabilities. This study further indicates that the emission band of the devices could be modified by changing the composition of emitting layer and therefore, OLEDs with different colors could be obtained.

4. Experimental

4.1. General procedure

All starting materials were purchased from Aldrich Chemical Co. ^{1}H and ^{13}C NMR spectra were recorded on the Bruker 300 MHz NMR spectrometers in $CDCl_3$. Thermogravimetric analyses (TGA) were performed on a Perkin–Elmer thermogravimeter (Pyris 1) under a dry nitrogen gas flow at the heating rate of 20 °C/min. Glass transition temperature (T_g) and melting point (T_m) of materials were determined by differential scanning calorimeter (DSC) of the Perkin–Elmer differential scanning calorimeter (DSC-7). The absorption spectra were recorded with the HP-8453A UV–Vis photodiode array spectrophotometer. The EL spectrum and the Commission Internationale de I'Eclairage (CIE) co-ordinates were measured by Pro-650 Spectroscanner, the current–voltage (I–V) characteristics were measured by Keithley 2400 Source meter. The highest occupied molecular orbital (HOMO) energy levels of organic materials were measured from the cyclic voltammetry (CV) [27] and the lowest unoccupied molecular orbital (LUMO) energy levels were determined from the HOMO energy levels and the optical band gap estimated from the absorption onset [28]. Photoluminescence (PL) was measured by Model LS 55 luminescence Spectrometer.

4.2. Synthesis

Ligands, 2-(2-quinolyl)naphtho[*b*]imidazole (QNI) and 2-(2-quinolyl)benzimidazole (QBI), were prepared as previously reported [29,30]. Complexes **1** and **2** were prepared in dry THF by reacting, in a 1:1.05 molar ratio, triphenylboron with QNI or QBI. The solutions were refluxed for 12 h under nitrogen. After the solvent was removed by vacuum, the residues were purified by a train sublimation method. Selected analytical data concerning complexes **1** and **2** are the following.

4.2.1. BPh_2(2-(2-quinolyl)naphtho[*b*]imidazolato) (**1**)

Pale yellow solid. 35% yield. M.p. >200 °C. ^{1}H NMR ($CDCl_3$, 293 K), δ ppm: 8.76 (d, 1H, $J = 8.7$ Hz, quinolyl), 8.70 (d, 1H, $J = 8.7$ Hz, quinolyl), 8.40 (s, 1H, imidazole), 8.37 (d, 1H, $J = 8.7$ Hz, quinolyl), 8.03 (dd, 1H, $J = 8.0$, 1.2 Hz, quinolyl), 7.96 (m, 1H, imidazole), 7.80 (m, 2H, imidazole and quinolyl), 7.67 (m, 2H, imidazole), 7.43 (m, 4H, ph), 7.32 (m, 2H, quinolyl), 7.24 (m, 6H, ph). MS data: 459.2 (35.13%), 382.1 (100%), 332.2 (61.62%), 295.2 (27.27%), 281.2 (20.64%), 267.2 (15.13%), 245.2 (11.05%), 229.5 (5.67%), 191.6 (19.73%), 152.8 (9.32%), 121.1 (14.23%), 104.1 (12.16%), 91.1 (9.51%), 73.1 (13.99%), 57.1 (14.51%). Anal. Calc. for $C_{32}H_{21}N_3B$ (MW = 459.2): C, 83.70; H, 4.83; N, 9.15. Found C, 83.64; H, 4.87; N, 9.12%.

4.2.2. BPh_2(2-(2-quinolyl)benzimidazolato) (**2**)

Pale yellow solid. 30% yield. M.p. >200 °C. ^{1}H NMR ($CDCl_3$, 293 K),δ ppm: 9.2 (d, 1H, $J = 6.3$ Hz, quinolyl), 8.67 (d, 1H, $J = 6$ Hz, imidazole), 8.35 (dd, 1H, $J = 6.3$, 1.2 Hz, quinolyl), 8.06 (d, 1H, $J = 6.6$ Hz, quinolyl), 7.82 (m, 2H, imidazole), 7.76 (m, 1H, imidazole), 7.28 (m, 3H, quinolyl), 7.20 (m, 10H, ph). MS data: 409.2 (13.36%), 382.5 (3.64%), 332.5 (100%), 331.5 (25.58%), 331 (1.57%), 295.4 (3.31%), 245.4 (2.72%), 205.2 (1.27%), 166.7 (1.25%), 151.3 (1.89%), 128.2 (2.41%), 77.1 (3.52%), 51.1 (1.52%). Anal. Calc. for $C_{28}H_{20}N_3B$ (MW = 409.2): C, 82.20; H, 4.89; N, 10.26. Found C, 82.14; H, 4.97; N, 10.26%.

4.2.3. Determination of the crystal structure

The diffraction data of complex **1** was collected on a Bruker AXS P4 diffractometer, which equipped with graphite-monochromated Mo Kα radiation ($\lambda = 0.71073$ Å). Structure refinements were carried out using the SHELXTL software package [31]. A pale yellow crystal

Table 2
Crystal data and structure refinement parameters for **1**

Empirical formula	$C_{33}H_{24}BCl_2N_3$
Formula weight	544.26
Temperature (K)	295(2)
Wavelength (Å)	0.71073
Crystal system	Monoclinic
Space group	$P2(1)/c$
Unit cell dimensions	
a (Å)	10.9609(12)
b (Å)	15.265(2)
c (Å)	16.646(2)
α (°)	90
β (°)	98.514(11)
γ (°)	90
Volume (Å^3)	2754.5(6)
Z	4
Calculated density (Mg m^{-3})	1.312
Absorption coefficient (mm^{-1})	0.264
$F(000)$	1128
Crystal size (mm)	$0.2 \times 0.6 \times 0.4$
Theta range for data collection (°)	1.82–25.00
Limiting indices	$-1 <= h <= 13$, $-18 <= k <= 1$, $-19 <= 1 <= 19$
Reflections collected	6034
Refinement method	Full-matrix least-squares on F^2
Data/restraints/parameters	4789/0/362
Goodness-of-fit on F^{-2}	1.191
Final R indices [$I > 2\sigma(I)$]	$R_1 = 0.0675$, $wR_2 = 0.1432$
R indices (all data)	$R_1 = 0.1368$, $wR_2 = 0.1688$
Largest difference peak and hole (e Å^{-3})	0.526 and −0.280

of **1** was mounted on the top of a glass fiber with epoxy cement. The unit cell constants were determined from reflections with θ in the range from 1.82° to 25.00°. The structure factors were obtained after Lorentz and polarization correction. The positions of some of the heavier atoms were located by the direct method. The remaining atoms were found in a series of alternating difference Fourier maps and least-square refinements. The final residuals of the final refinement were $R_1 = 0.0675$, $wR_2 = 0.1432$. Selected bond distances and angles are listed in Table 1, and basic information pertaining to crystal parameters and structure refinement is summarized in Table 2.

5. Supplementary material

Crystallographic data for the structural analysis has been deposited with the Cambridge Crystallographic Data Centre as supplementary publication nos. CCDC 281876. Copies of the data can be obtained, free of charge, on application to CCDC, 12 Union Road, Cambridge CB2 1EZ, UK (fax: +44 0 1223 336033 or e-mail: deposit@ccdc.cam.ac.uk).

Acknowledgement

We thank the National Science Council of the Republic of China for financial support.

References

[1] D. Song, S.F. Liu, R.Y. Wang, S. Wang, J. Organomet. Chem. 631 (2001) 175.
[2] Q. Liu, M.S. Mudadu, H. Schmider, R. Thummel, Y. Tao, S. Wang, Organometallics 21 (2002) 4743.
[3] J.E. Lee, G.C. Choi, B.O. Rim, S.M. Kim, N.G. Park, Y.K. Ha, Y.S. Kim, Mater. Sci. Eng. C 24 (2004) 269.
[4] C.W. Tang, S.A. VanSlyke, Appl. Phys. Lett. 51 (1987) 913.
[5] C. Adachi, S. Tokito, J. Tsutusi, S. Saito, Jpn. J. Appl. Phys. 27 (1998) 713.
[6] J.H. Burroughes, D.D.C. Bradley, A.R. Brown, R.N. Marks, K. Mackay, R.H. Friend, P.L. Burns, A.B. Homes, Nature 347 (1990) 539.
[7] J.R. Sheats, H. Antoniadis, M. Hueschen, W. Leonard, J. Miller, R. Moon, D. Roitman, A. Stocking, Science 273 (1996) 884.
[8] H. Nakada, T. Tohma, Inorganic and Organic Electroluminescence, Wissenschaft-und-Technik-Verlag, Berlin, 1996, p. 385.
[9] S.F. Liu, C. Seward, H. Aziz, N.X. Hu, Z. Popovic, S. Wang, Organometallics 19 (2000) 5709.
[10] H. Schmidbaur, J. Lettenbauer, D.L. Wilkinson, G. Muller, O.Z. Kumberger, Naturforsch 46B (1991) 901.
[11] R. Balamurugan, M. Palaniandavar, Inorg. Chem. 40 (2001) 2246.
[12] Z.K. Chen, H. Meng, Y.H. Lai, W. Huang, Marcromolecules 32 (1999) 4351.
[13] S. Tokito, H. Tanaka, K. Noda, A. Okada, Y. Taga, Appl. Phys. Lett. 70 (1997) 1929.
[14] J.H. Kim, M. Matsuoka, K. Fukunishi, Dyes Pigments 40 (1998) 53.
[15] F. Peral, E. Gallego, J. Mol. Struct. 372 (1995) 101.
[16] A. Sarkar, S. Chakravorti, J. Lumin. 65 (1995) 163.
[17] Y.V. Ilichev, W. Kuhnle, K.A. Zachariasse, J. Chem. Phys. 211 (1996) 441.
[18] A.A. Ibrahim, Bull. Soc. Chim. Fr. 134 (1997) 593.
[19] M. La Deda, M. Ghedini, I. Aiello, T. Pugliese, F. Barigelletti, G. Accorsi, J. Organomet. Chem. 690 (2005) 857.
[20] I. Aiello, M. Ghedini, M. La Deda, J. Lumin. 96 (2002) 249.
[21] N.G. Park, J.E. Lee, Y.H. Park, Y.S. Kim, Synth. Met. 145 (2004) 279.
[22] K.Y. Ho, W.Y. Yu, K.K. Cheung, C.M. Che, Chem. Commun. (1998) 2101.
[23] R. Aroca, T.D. Cano, Chem. Mater. 15 (2003) 38.
[24] H. Beens, A. Weller, in: J.B. Birks (Ed.), Organic Molecular Photophysics, vol. 2, Wiley, New York, 1975, p. 159.
[25] J. Kido, M. Kimura, K. Nagai, Science 267 (1995) 1332.
[26] C.W. Tang, S.A. VanSlyke, C.H. Chen, J. Appl. Phys. 65 (1987) 3610.
[27] D. Kolosov, V. Adamovich, P. Djurovich, M.K. Thompson, C. Adachi, J. Am. Chem. Soc. 124 (2002) 9945.
[28] H. Ishii, K. Sugiyama, E. Ito, K. Seki, Adv. Mater. 11 (1999) 605.
[29] T.R. Chen, J. Mol. Stuct. 737 (2005) 35.
[30] T.R. Chen, A. Yeh, J.D. Chen, Tetrahedron Lett. 46 (2005) 1569.
[31] SHELXTL 5.10. Bruker Analytical X-ray Instruments Inc., Karlsruche, Germany, 1997.